SUPPLEMENTARY DATA

SUPPLEMENTARY MATERIAL

Isometric Force Measurements

Standard organ baths techniques were used to measure contractile activity in strips of wild-type and *Lep*^{ob} antrum. Muscle strips were cut parallel to the circular layer and attached, via fine silk suture thread, to an isometric force transducer (Fort10g, World Precision Instruments, Sarasota, FL) at one end and to a fixed support at the other. The strips were placed in organ baths that were continually perfused with oxygenated KRB maintained at 37°C. Passive tension of 2-3mN was applied to the antral muscle strips. The muscle strips were allowed to equilibrate in the organ baths for 1hr during which spontaneous, rhythmic contractions developed.

Video Imaging of Gastric Peristalsis

Antral muscle sheets were pinned flat to the base of a Sylgard elastomer (Dow Corning Corp, Midland, MI) coated dish, circular muscle layer facing upwards. Gastric muscles were perfused with oxygenated KRB at 37°C. The recording and analysis of videos has previously been described (1). In brief, antral movements were monitored by video recordings (4min; Fig. 1*C*), using a high-definition video camera (DMK 31AF03, ImagingSource, Charlotte, NC) and AstroIIDC software (ASC, Calgary, Alberta, Canada). Peristaltic contractions resulted in indentations of the muscle sheet edges, which could be detected and used to produce spatiotemporal maps using Volumetry software (Grant Hennig; Supplementary Fig. 1*D* and *E*). The process by which Volumetry generates spatiotemporal maps from video recordings has been detailed previously (1). Edge tracking techniques and black markers placed on the surface of the muscles were used to track muscle contractions. The frequency and amplitude (i.e. contractile displacement) of antral contractions were calculated from the spatiotemporal maps.

Immunohistochemistry

Whole mounts of gastric antrum were stretched to 110 % of resting length and width before being fixed in paraformaldehyde (4% w/v; 10min; 4^{o}C). Tissues were washed overnight in phosphate buffered saline (PBS; 0.01M, pH7.2) and incubated in bovine serum albumin (BSA; 1%, 1.5hr, room temperature) to reduce non-specific antibody binding. Primary antibody incubations were for 48h, 4°C (see Supplemental Table 1 for antibody details), diluted in 0.5% Triton-X 100. Tissues were washed with PBS (4x1hr). Immunoreactivity was detected using the appropriate Alexa Fluor 488 antibodies (1:1,000 in PBS; 1hr, room temperature). Control tissues were prepared by omitting either primary or secondary antibodies from the incubation solution. After washing with PBS (overnight, 4°C), whole mounts were mounted on glass slides and examined with an LSM 510 Meta confocal microscope (Zeiss, Oberkochen, Germany). Images were then deconvolved (AutoQuantX, MediaCybernetics, MD). Confocal micrographs are digital composites of image stacks that were constructed using Zeiss LSM 5 Image Examiner software and converted to TIFF files.

Western Analysis

Total protein was extracted from *Lep*^{ob} and wild-type antral muscles. Protein concentration of isolated muscle extracts was determined by the Bradford assay (Bio-Rad, Richmond, CA). A total of 30µg of protein from each lysate was used for the blot. Proteins were subjected to 10% SDS-PAGE, transferred to a nitrocellulose membrane and probed with the primary antibodies listed in supplemental Table 2. After washing, the blot membrane was incubated with alkaline phosphatase-conjugated immunoglobulin G secondary antibody (Santa Cruz Biotechnology, Inc., Dallas, Texas). After another wash, the color development by NBT/BCIP (Roche Diagnostics, Mannheim, Germany) was stopped. The amount of proteins on the blot was analyzed using Quantity One 4.5.1 software (Bio-Rad, Hercules, California). ImageJ software (NIH, Bethesda, MD) was used to calculate the relative densities of protein compared with housekeeper glyceraldehyde 3-phosphate dehydrogenase (GAPDH).

SUPPLEMENTARY DATA

RNA Isolation and Real-Time Quantitative PCR

Total RNA was isolated from the tunica muscularis of *Lep*^{ob} and wild-type antrums (following removal of the mucosa and submucosa) using TRIzol Reagent (Invitrogen, Carlsbad, CA) as per the manufacturer's protocol; tissues were homogenized using a tissue grinder and 21-gauge sterile syringe during the lysis phase of the protocol. Final product was eluted with 25µl diethylpyrocarbonate (DEPC)-treated water. Concentration and purity of RNA was measured using a ND-1000 Nanodrop Spectrophotometer (Nanodrop, Wilmington, DE). First strand cDNA was synthesized from 100ng of each RNA using qScript™ cDNA SuperMix (Quanta Biosciences, Gaithersburg, MD) in a 5X reaction buffer containing optimized concentrations of $MgCl_2$, dNTPs (dATP, dCTP, dGTP, dTTP), recombinant RNase inhibitor protein, qScript reverse transcriptase, random primers, oligo(dT) primer and stabilizers. This was followed by heat inactivation. Primers were designed to investigate the expression of various components of the prostaglandin synthesis pathway and prostaglandin receptors (see supplemental Table 3 for primer details). Quantitative PCR (qPCR) was performed with the same primers used for PCR using SYBR green chemistry on the 7900 HT Real Time PCR System (Applied Biosystems, Carlsbad, CA). cDNA was prepared from four wild-type and four *Lep*^{ob} antrums and each cDNA was tested in triplicate replicates. Negative (no template) controls were included in each qPCR run. Melting curve analysis was performed using the manufacturer's standard protocol with no evidence for primer dimer or nonspecific products. Regression analysis using the serial 10-fold dilutions cDNA was used to generate standard curves. Unknown amounts of messenger RNA (mRNA) were plotted relative to the standard curves for each set of primers and graphically plotted using Microsoft Excel. A regression line with a correlation coefficient (R^2 value) of >0.98 and primer efficiencies of 95-105% were only accepted for analysis. This gave transcriptional quantification of each gene relative to GAPDH standard after log transformation of the corresponding raw data. Differences between normalized wild-type and *Lep*^{ob} samples were assessed using a Students t-test assuming unequal variance (P>0.05).

Solutions and Drugs

Recording chambers for physiological experiments were perfused with KRB containing (in mmol/L): NaCl, 120.35; KCl, 5.9; $NaHCO_3$, 15.5; NaH_2PO_4, 1.2; $MgCl_2$, 1.2; $CaCl_2$, 2.5; and glucose, 11.5. The pH of the KRB was maintained at 7.3-7.4 when bubbled with 97% O_2-3% CO_2 at 37±0.5°C. After pinning, antral tissues were left to equilibrate for 1hr before experiments were started. Valdecoxib (Tocris Bioscience, Bristol, UK) was used to inhibit PTGS2 and was dissolved in DMSO at a stock concentration of 10mM before being added to KRB and perfused at a final concentration of 1µM.

Statistical Analysis

Significance was calculated by appropriate statistical tests. Data are expressed as means±SD. The use of "n" refers to the number of animals utilized. *P* values <0.05 were considered statistically significant. In figures, *, **, ***, **** represent $P \leq 0.05$, $P \leq 0.01$, $P \leq 0.001$, $P \leq 0.0001$, respectively. GraphPad Prism 7 was used for analysis and graph production (GraphPad Software, Inc., La Jolla, CA). All figures were arranged using Corel Draw X4 (Corel Corp., Mountain View, CA).

SUPPLEMENTAL DATA

Post-junctional neural responses in gastric antrums of *Lep*^{ob} animals

Enteric inhibitory neural responses in antrums of mice consist predominantly of a fast-purinergic inhibitory junction potential (IJP) (25). Single pulses (0.3ms duration) caused IJP amplitudes averaging 12±2.0mV with a half-maximal duration of 0.7±0.2s in wild-type mice (Supplementary Fig. 2*A*, *C* and *D*; *n*=3) and 11±2.0mV with a half-maximal duration of 0.57±0.1s in *Lep*^{ob} antral muscles (Supplementary Fig. 2*B*, *C* and *D*; *n*=5). Stimulating at 10Hz (0.3ms;1s) caused IJPs averaging 11±1.0mV with half-durations of 1.7±0.4s in wild-type mice (Supplementary Fig. 2*A*, *C* and *D*; *n*=4) and 10±4.0mV with half-durations of 1.5±0.1s in *Lep*^{ob} mice (Fig. 2*B*, *C* and *D*; *n*=5). Thus, significant

SUPPLEMENTARY DATA

differences in post junctional neural responses were not detected in *Lep*^{ob} antrums. However, since antrums of *Lep*^{ob} mice were depolarized by 6 mV compared to controls, the amplitude of IJPs in *Lep*^{ob} tissues could be considered to be reduced.

Supplementary Figure 1. Disrupted antral propagating motor patterns in *Lep*^{ob} gastric antrums. *A*: Image of intact stomach with gastric anatomical regions indicated (LC and GC stand for lesser curvature and greater curvature, respectively). The method of dissection of the stomach is marked by the dashed line and scissors. The stomach was cut open along the lesser curvature and the fundus removed. *B:* The muscle sheet was then pinned flat and the mucosa removed by sharp dissection. Black markers were placed on the surface of the circular muscle to allow monitoring of gastric wall contractions. The vertical dashed line indicates the axis of the greater curvature, while the horizontal dashed line and scissors indicates where corpus and antrum were separated. *C*: Image of the preparation after corpus and antrum were dissected apart (Scale bar in *A* applies to panels *A*-*C*). *D* and *E*: Video recordings, 4 minutes in length, were made in order to observe the contractile activity of the muscle sheet. Spatiotemporal maps were generated from antral regions by tracking indentation of muscle edges, during circular muscle contractions. Each contraction produces a vertical black band on the spatiotemporal map. Left to right on each spatiotemporal map represents time, while top to bottom represents space (proximal antrum to distal antrum). *D:* A spatiotemporal map generated from the antral region of a wild-type mouse showing robust contractions at a frequency of 4min^{-1}. *E*: A spatiotemporal map from the antrum of a *Lep*^{ob} mouse; contractions were much weaker than wild-type control, producing small movements and therefore only faint vertical black bands were observed (apart from one intense contraction towards the end of the 4-minute recording). The weaker contractions of the *Lep*^{ob} antrum occurred at 6 min^{-1}.

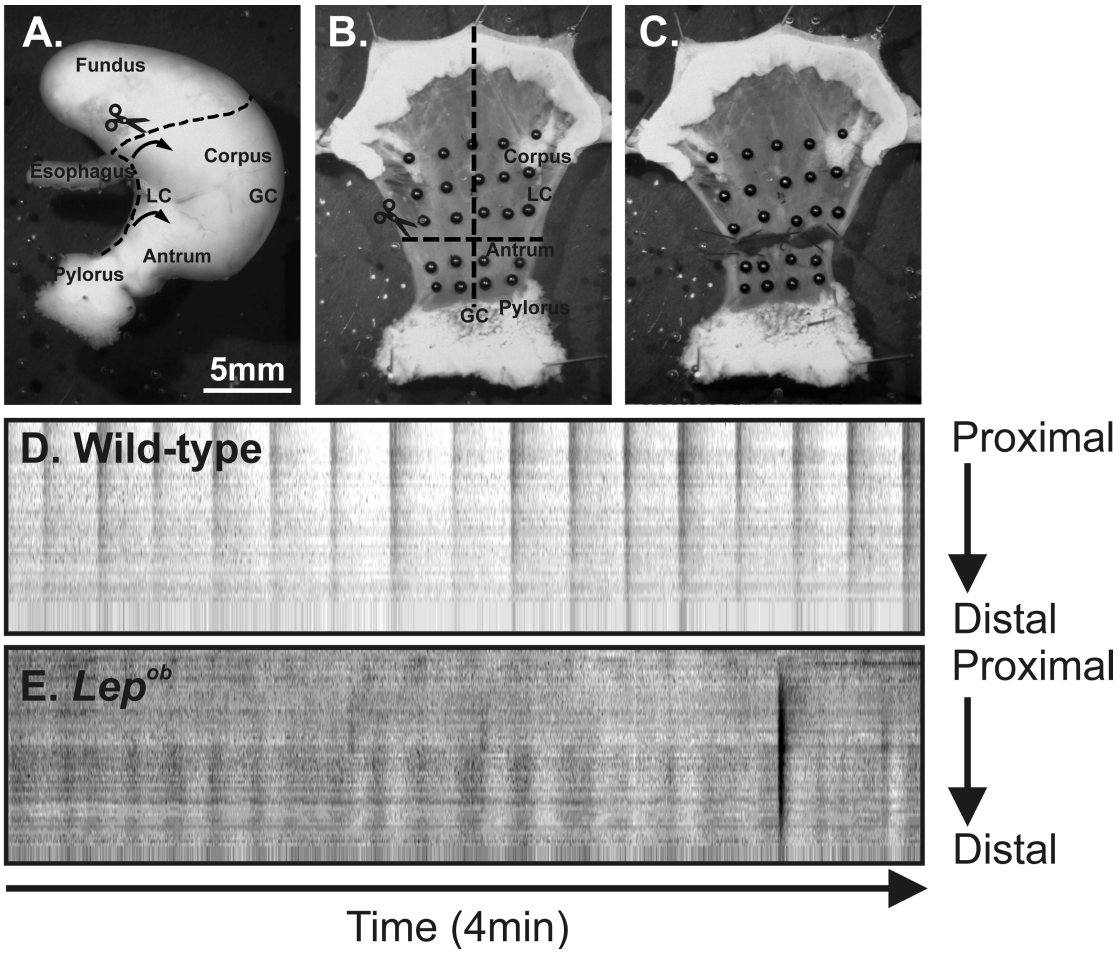

SUPPLEMENTARY DATA

Supplementary Figure 2. Post-junctional neural responses were unaffected in *Lep*^{ob} antrums compared to wild-type controls. *A:* Typical post-junctional neural responses to electrical field stimulation (EFS; 0.3ms duration pulses delivered at 1Hz (arrow) and 10Hz (horizontal bar) for 1 second) consisted of membrane hyperpolarization termed an inhibitory junction potential (IJP). *B:* In *Lep*^{ob} antrums, EFS evoked IJPs that were similar in amplitude and half-maximal duration as controls. *C* and *D:* Summarized data showing no statistical difference in inhibitory neural responses between wild-type control (white bars) and *Lep*^{ob} antrums (black bars) (unpaired Student's *t*-test).

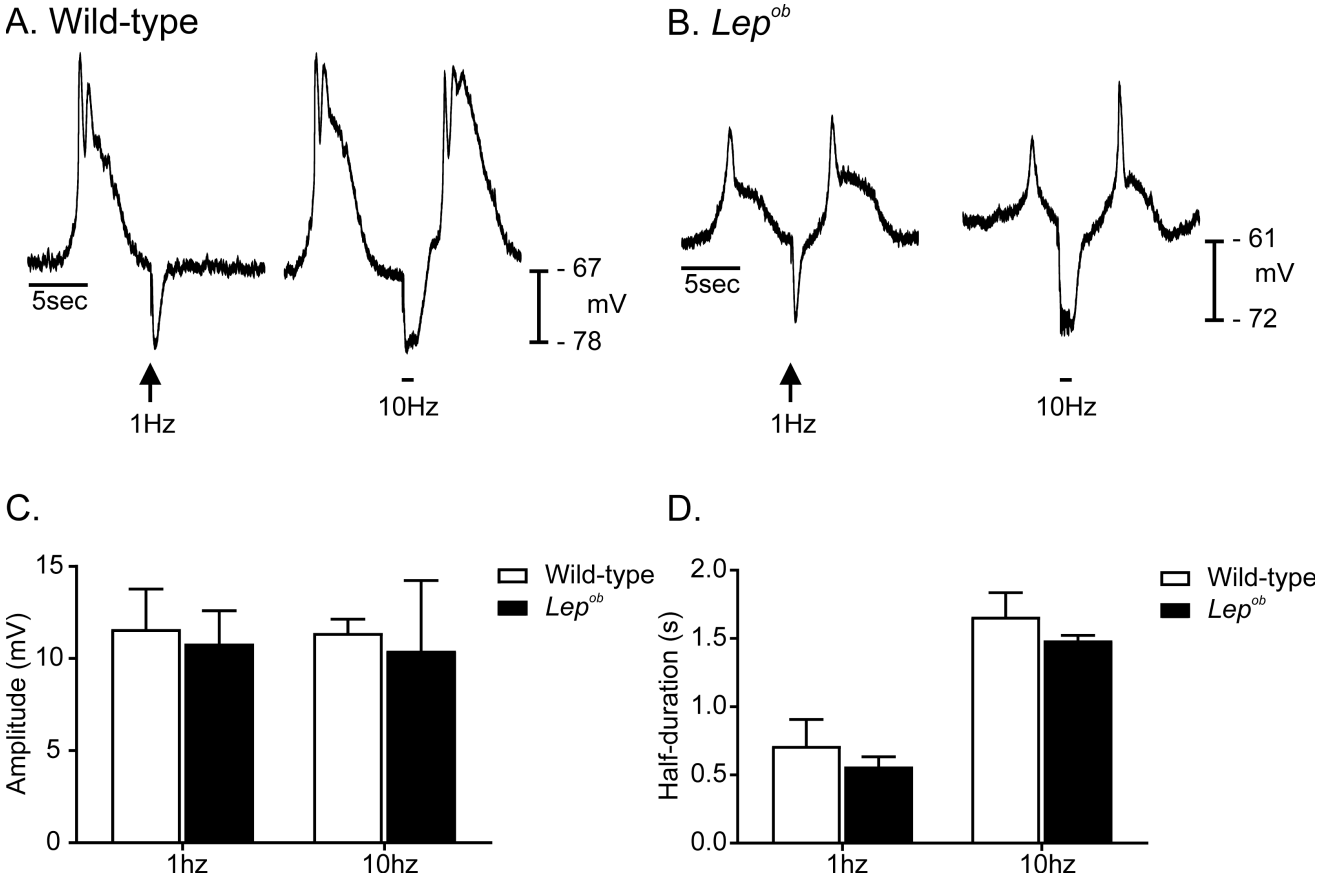

SUPPLEMENTARY DATA

Supplementary Figure 3. Summarized slow wave parameters from 9 intracellular recording sites of antrums from wild-type controls and *Lep*^{ob} animals. *A:* Slow wave frequency showing statistically significant differences in most regions of *Lep*^{ob} (black bars) compared to wild-type animals (white bars). *B:* Slow waves amplitudes were also significantly smaller in most regions of the gastric antrums of *Lep*^{ob} animals compared to wild-type controls (unpaired Student's t-test).

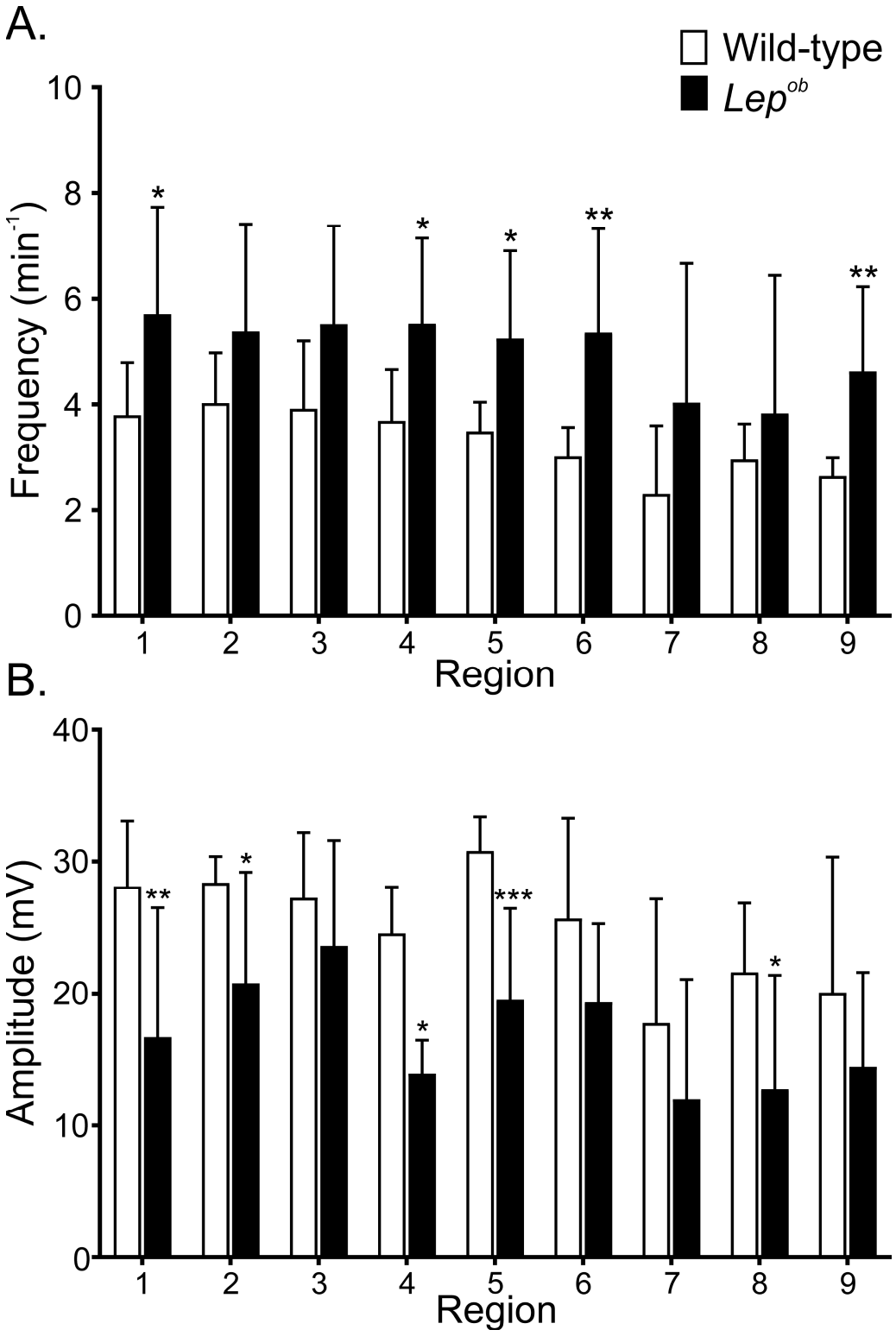

SUPPLEMENTARY DATA

Supplementary Figure 4. Networks of ICC, NOS1$^+$ nerves and PDGFRA$^+$ cells along the lesser curvature of antrums from *Lep^{ob}* and wild-type animals. *A-D:* Representative images of ICC, *E-H:* NOS1$^+$ neurons and *I-L:* PDGFRA$^+$ cells. *A*, *E* and *I* show ICC, NOS1$^+$ nerve fibers and PDGFRA$^+$ cells, respectively, within the circular muscle layer of a wild-type antrum; *C*, *G* and *K* show ICC, NOS1$^+$ nerve fibers and PDGFRA$^+$ cells, respectively, within the circular muscle layer of a *Lep^{ob}* antrum. *B*, *F* and *J* show ICC, NOS1$^+$ neurons and PDGFRA$^+$ cells, respectively, in the myenteric plexus region of a wild-type antrum. *D*, *H* and *L* show ICC, NOS1$^+$ neurons and PDGFRA$^+$ cells, respectively, in the myenteric plexus region of a *Lep^{ob}* antrum. Scale bar in *L* applies to all panels.

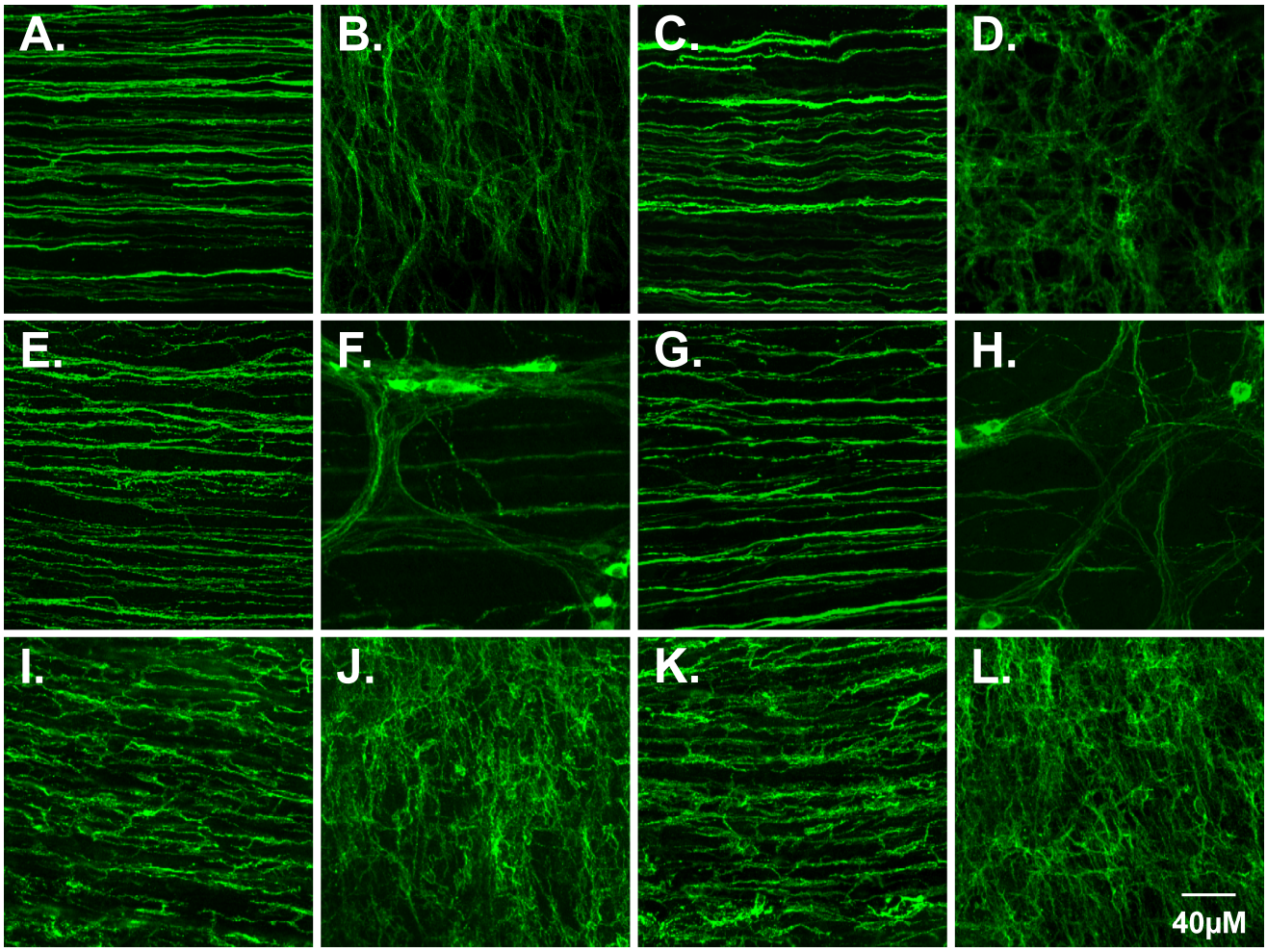

SUPPLEMENTARY DATA

Supplementary Figure 5. PTGS2 inhibition normalizes phasic contraction force and frequency and restores motility patterns of *Lep*^{ob} antrums. *A* and *B:* Phasic contractile activity of the circular layer of a *Lep*^{ob} antrum before (*A*) and after (*B*) valdecoxib (1 μM). *C* and *D:* Summary of the changes in frequency (C) and isometric force (D) of phasic antral contractions of *Lep*^{ob} muscles before and after valdecoxib. *E-H:* In comparison, phasic contractions of the circular layer of a wild-type antrum before (*E*) and after (*F*) valdecoxib. *G* and *H:* Summarized data of the changes in frequency (G) and contractile force (H) of wild-type controls before and after valdecoxib. Note that changes of *Lep*^{ob} antrums were significantly greater than wild-type controls. Statistically significant changes are indicated (paired Student's *t*-test). *I* and *J:* Spatiotemporal maps show normalization of gastric antrum motility patterns of a *Lep*^{ob} antrum after valdecoxib (1 μM). Spatiotemporal map of *Lep*^{ob} antrum prior to (*I*) and after (*J*) addition of valdecoxib (1μM). Note this map was from the same recording shown in figure 1.

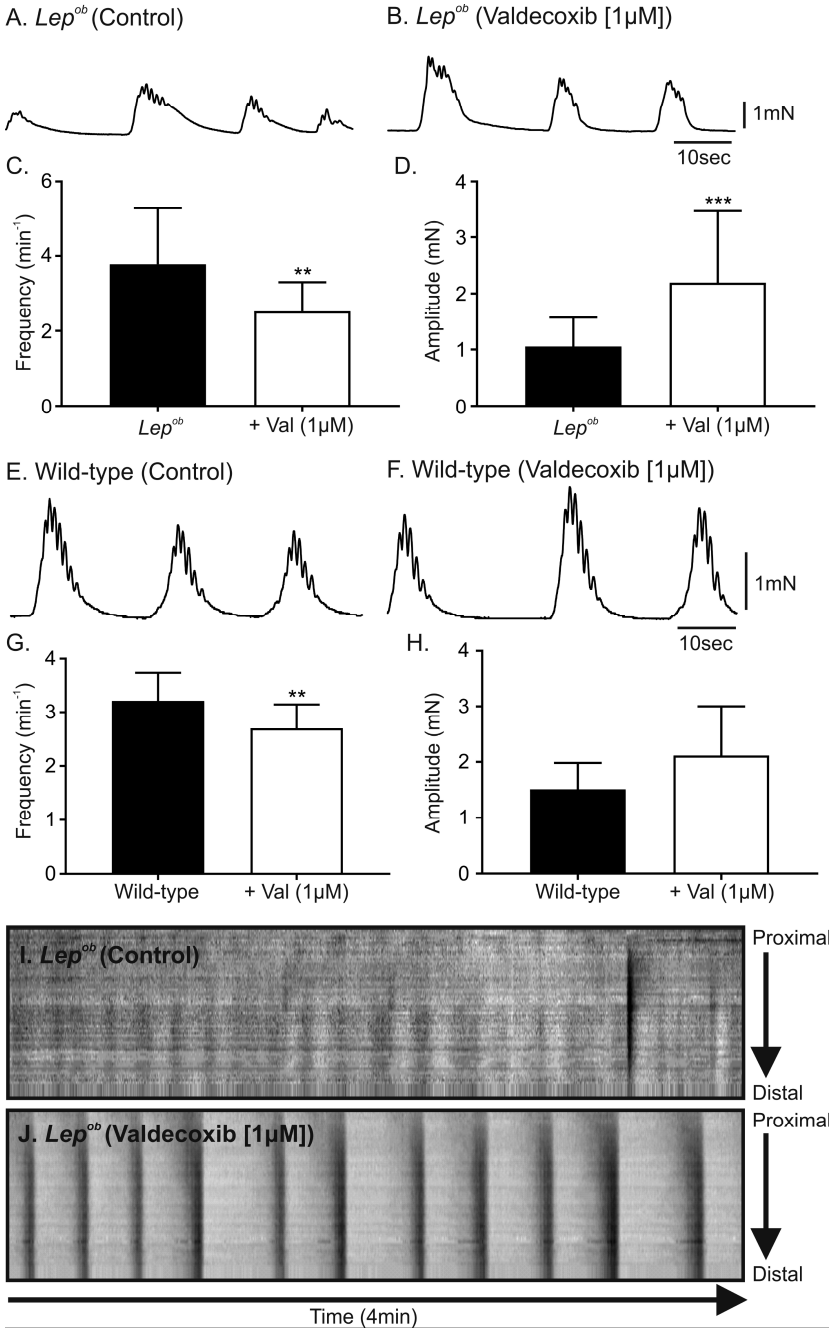

SUPPLEMENTARY DATA

SUPPLEMENTARY REFERENCES

1. Forrest AS, Hennig GW, Jokela-Willis S, Park CD, Sanders KM. Prostaglandin regulation of gastric slow waves and peristalsis. Am J Physiol Gastrointest Liver Physiol. 2009;296(6):G1180-90.

Supplementary Table 1. Details of Primary Antibodies Used for Immunohistochemistry

Antibodies	Resource	Mono- or poly-clonal antibodies	Host	Dilution
Anti-mSCF-R	R&D Systems Inc., Minneapolis, MN, USA	Poly	goat	1:500
Anti-NOS1	Santa Cruz Biotechnology, Inc., Santa Cruz, CA, USA	Poly	Rabbit	1:500
Anti-mPDGFRα	R&D Systems Inc., Minneapolis, MN, USA	Poly	goat	1:100

Note: mSCF-R: mouse stem cell factor receptor; mPDGFRα: mouse platelet derived growth factor receptor α; NOS1: nitric oxide synthase 1.

Supplementary Table 2. Details of Antibodies Used for Western Blots

Antibodies	**Resource**
GAPDH	Santa Cruz Biotechnology, Inc., Santa Cruz, CA, USA
mSCF-R	R&D Systems Inc., Minneapolis, MN, USA
UCHL1	UltraClone Limited, Isle of Wight, England, UK
NOS1	Gift from Dr. Piers Emson, Molecular Science Group, Cambridge, UK
SNAP25	Covance, Princeton, NJ, USA
Syntaxin	Sigma-Aldrich, Saint Louis, MO, USA
DLG4	Millipore, Billerica, MA, USA
MYH11	Biomedical Technologies, Stoughton, MA, USA

Note: GAPDH: Glyceraldehyde 3-phosphate dehydrogenase; mSCF-R: mouse stem cell factor receptor; UCHL1: ubiquitin carboxy-terminal hydrolase L1; NOS1: nitric oxide synthase 1; SNAP-25: Synaptosomal-associated protein-25; DLG4: Discs Large MAGUK Scaffold Protein 4; MYH11: myosin heavy chain 11.

SUPPLEMENTARY DATA

Supplementary Table 3. Accession Numbers and Primers Used For qPCR

Target Transcript	Accession numbers	Oligonucleotide sequences (5′-3′)
GAPDH	NM_008084.2	GCCGATGCCCCCATGTTTGTGA (F) GGGTGGCAGTGATGGCATGGAC (R)
Ptger1	NM_013641.2	GCCTCGTCTGCCTCATCCATCACT (F) TGGCCAACACCACCAACACCAG (R)
Ptger2	NM_008964.4	CTGGATCTCGCAGGAGAGGAGAGAGGA (F) GCTCGGAGGTCCCACTTTTCCTTTAGG (R)
Ptger3	NM_011196.2	AATCACCACGGAGACGGCCATCCAG (F) GCGAAGCCAGGCGAACTGCAATTAGA (R)
Ptger4	NM_001136079.1	CGGGTGCGGAGATCCAGATGGTCAT (F) GGCCTGCAAATCTGGGTTTCTGCTGA (R)
Ptgfr	NM_008966.3	GTGCAATGCCGTCACGGGAG (F) TTGTTACCAGAAAGGGACTCCAGCA (R)
Ptgir	NM_008967.3	CTCCCTGCCTCTCATGATCCG (F) CAGGGGTCCAGGATGGGGTTG (R)
Ptgr1	NM_025968.3	CGAGCAAGTGGCCAGAGTCG (F) GTCCGGCCACTCTACAGGCA (R)
Hpgd	NM_008278.2	TTAGCAGGGCTCATGCCTGTTGC (F) TGTGTCCACAAAGCCTGGGCA (R)
Ptges1	NM_022415.3	TGCCTCAGAGCCCACCGCAA (F) GGAGCGAAGGCGTGGGTTCA (R)
Ptgs1	NM_008969.3	GCCTTAGGCCCACGGGGTAGAC (F) CGCATCAACACGGACGCCTG (R)
Ptgs2	NM_011198.3	GATGCTCTTCCGAGCTGTGCTG (F) CATAGAATCCAGTCCGGGTACAGTC (R)

Note: GAPDH: Glyceraldehyde 3-phosphate dehydrogenase; Ptger1: prostaglandin E receptor 1 (EP1); Ptger2: prostaglandin E receptor 2 (EP2); Ptger3: prostaglandin E receptor 3 (EP3); Ptger4: prostaglandin E receptor 4; Ptgfr: prostaglandin F receptor (FP); Ptgir: prostaglandin I receptor (IP); Ptgr1: prostaglandin reductase 1; Hpgd: hydroxyprostaglandin dehydrogenase 15-(NAD); Ptges1: microsomal prostaglandin E synthase 1; Ptgs1: prostaglandin-endoperoxide synthase 1 (COX1); Ptgs2: prostaglandin-endoperoxide synthase 2 (COX2). (F): forward primer; (R): reverse primer.

SUPPLEMENTARY DATA

Supplementary Table 4. Mean Amplitude and Frequency Values From All 9 Antral Regions in Both Wild-Type and *Lep*^{ob} Mice

	Amplitude (mV)		Frequency (min^{-1})	
Region	**Control**	***Lep*^{ob}**	**Control**	***Lep*^{ob}**
1	28.1 ± 4.9 (9)	16.7 ± 9.8 (9)	3.8 ± 1.0 (8)	5.7 ± 2.0 (9)
2	28.3 ± 2.0 (8)	20.8 ± 8.4 (9)	4.0 ± 0.9 (8)	5.4 ± 2.0 (9)
3	27.2 ± 4.9 (8)	23.6 ± 8.0 (9)	3.9 ± 1.3 (8)	5.5 ± 1.9 (9)
4	27.3 ± 6.6 (7)	14.0 ± 7.1 (8)	3.7 ± 1.0 (8)	5.5 ± 1.6 (8)
5	30.8 ± 2.6 (9)	19.5 ± 6.9 (9)	3.5 ± 0.6 (8)	5.2 ± 1.7 (9)
6	28.0 ± 4.3 (7)	21.1 ± 2.9 (8)	3.0 ± 0.6 (8)	5.4 ± 2.0 (9)
7	17.8 ± 9.4 (6)	12.0 ± 9.0 (7)	2.3 ± 1.3 (6)	4.0 ± 2.6 (7)
8	21.6 ± 5.2 (7)	12.8 ± 8.6 (8)	3.0 ± 0.7 (7)	3.8 ± 2.6 (8)
9	20.1 ± 10.3 (7)	14.5 ± 7.1 (6)	2.6 ± 0.3 (7)	4.6 ± 1.6 (6)

Note: Values = Mean ± SD; *n* numbers in parentheses.